



HAL
open science

Interaction of D₂ with H₂O amorphous ice studied by temperature-programed desorption experiments

L. Amiaud, J. H. Fillion, S. Baouche, F. Dulieu, A. Momeni, J. L. Lemaire

► **To cite this version:**

L. Amiaud, J. H. Fillion, S. Baouche, F. Dulieu, A. Momeni, et al.. Interaction of D₂ with H₂O amorphous ice studied by temperature-programed desorption experiments. *Journal of Chemical Physics*, 2006, 124 (9), pp.094702. 10.1063/1.2168446 . hal-02163766

HAL Id: hal-02163766

<https://hal.science/hal-02163766>

Submitted on 24 Jun 2019

HAL is a multi-disciplinary open access archive for the deposit and dissemination of scientific research documents, whether they are published or not. The documents may come from teaching and research institutions in France or abroad, or from public or private research centers.

L'archive ouverte pluridisciplinaire **HAL**, est destinée au dépôt et à la diffusion de documents scientifiques de niveau recherche, publiés ou non, émanant des établissements d'enseignement et de recherche français ou étrangers, des laboratoires publics ou privés.

Interaction of D₂ with H₂O amorphous ice studied by temperature-programmed desorption experiments

L. Amiaud, J. H. Fillion,^{a)} S. Baouche, F. Dulieu, A. Momeni, and J. L. Lemaire
 LERMA-LAMAp, CNRS UMR 8112, Université de Cergy-Pontoise et Observatoire de Paris,
 5 Mail Gay-Lussac, F-95031 Cergy-Pontoise Cedex, France

(Received 17 November 2005; accepted 23 December 2005; published online 1 March 2006)

The gas-surface interaction of molecular hydrogen D₂ with a thin film of porous amorphous solid water (ASW) grown at 10 K by slow vapor deposition has been studied by temperature-programmed-desorption (TPD) experiments. Molecular hydrogen diffuses rapidly into the porous network of the ice. The D₂ desorption occurring between 10 and 30 K is considered here as a good probe of the effective surface of ASW interacting with the gas. The desorption kinetics have been systematically measured at various coverages. A careful analysis based on the Arrhenius plot method has provided the D₂ binding energies as a function of the coverage. Asymmetric and broad distributions of binding energies were found, with a maximum population peaking at low energy. We propose a model for the desorption kinetics that assumes a complete thermal equilibrium of the molecules with the ice film. The sample is characterized by a distribution of adsorption sites that are filled according to a Fermi-Dirac statistic law. The TPD curves can be simulated and fitted to provide the parameters describing the distribution of the molecules as a function of their binding energy. This approach contributes to a correct description of the interaction of molecular hydrogen with the surface of possibly porous grain mantles in the interstellar medium. © 2006 American Institute of Physics. [DOI: 10.1063/1.2168446]

I. INTRODUCTION

Amorphous solid water (ASW) has received great attention because of its fundamental analogy with liquid water at low pressure^{1,2} and because water is a major component of ices observed in low-temperature astrophysical environments³ such as the interstellar medium (ISM), protoplanetary disks, planetary bodies, and cometary nuclei.

In dense (10^4 – 10^8 cm⁻³ hydrogen atoms) and cold (10–90 K) molecular clouds, silicate and carbonaceous dust particles are presumed to be covered with molecular ices consisting mainly of H₂O and other organic molecules.^{4,5} The surface layer of the grain mantles are grown by accretion of atoms and molecules from the interstellar gas and by subsequent reactions that can also form complex organic species.⁵ These ices can be processed by cosmic ray impact, ultraviolet photolysis, and shocks. The Infrared Space Observatory (ISO) has contributed greatly to the observation of interstellar ices in the environment of dense clouds.^{6,7} The physical structure and the chemical composition of interstellar ices are dependent on the pressure, gas-phase composition, temperature, and gravitational conditions encountered in these regions. Although the various forms possible for such water-rich ices grown under interstellar conditions are not precisely known, amorphous forms are likely to play an important role.^{8–11} For example, the 3.07 μm interstellar absorption band is consistent with laboratory observations of pure amorphous ice sample at 10 K.¹⁰ In the interstellar medium, the interaction of the gas with ASW is therefore ex-

pected to play a key role in the chemical evolution of dense interstellar regions. Among the gas-phase species, molecular hydrogen is of fundamental astrophysical relevance. This molecule, which is a central species in interstellar chemistry, dominates the composition of the molecular clouds and thereby their dynamics.

In the laboratory, ASW can be obtained under high-vacuum conditions by slow vapor deposition (typically <0.5 ML/s) onto a cold substrate. It is known that amorphous ice is formed below 130 K, while cubic crystalline ice (*I_c*) is formed between 130 and 160 K and hexagonal crystalline ice (*I_h*) is obtained above 160 K. Other amorphous phases of H₂O ice that are produced by compressing (at low temperature) stable crystalline phases or by condensation from existing supercooled liquid droplets are not concerned by the present study.

ASW can be grown with various porosities, depending on the impinging flux, substrate temperature, and deposition technique.^{12–15} In particular, discrepancies in experiments conducted by different groups can be solved by considering that the direction of incidence of the water molecules onto the surface can affect the morphology of the sample.¹⁶ Temperature-programmed-desorption (TPD) experiments monitoring well-collimated molecular-beam deposition processes have demonstrated that the properties of ASW grown by vapor condensation depend on the angular distribution of the water molecule impinging from the gas phase.^{17–19} By deposition at low temperature (<90 K), nonporous to highly porous ASW films could be grown, with apparent surface areas as high as few thousands m²/g. Ballistic deposition simulations²⁰ that qualitatively reproduce the above results

^{a)}Author to whom correspondence should be addressed. Electronic mail: jean-hugues.fillion@obspm.fr

provide a picture of the ice morphology presenting a network of nanometric voids that are partly connected together and open to the external surface. The apparent surface areas of the ice films decrease with increasing growth temperature. This effect has been related to the collapse of the voids. Films annealed up to a given temperature are, however, not equivalent (more porous) than films grown at that same temperature.¹⁸ The average density values obtained by optical interference measurements²¹ are also consistent with an increasing porosity for ices grown at very low temperature. Finally, it has to be kept in mind that films grown by background dosing (e.g., by introducing water vapor to the vacuum chamber through a leak valve) and at very low temperature are found to be highly porous.

Electron-diffraction and x-ray measurements have revealed distinct structures of ASW.^{8,22,23} At very low temperature ($T < 30$ K), the diffraction patterns closely resemble those of high-density amorphous ice (HDA), which is formed by pressurization of (I_h).^{8,23} High-density amorphous ice and amorphous ice prepared at low temperature are, however, not equivalent.^{24,25} Between 38 and 68 K, ASW undergoes an irreversible and gradual conversion towards another form characterized by a diffraction pattern more similar to the low-density amorphous ice (LDA),²⁶ which is grown around 77 K at atmospheric pressure. Molecular-dynamics calculations indicate that the resulting ice is best described by an imperfect random network of hydrogen bonds (“H bonds”), contrary to the crystalline cubic ice in which each water molecule forms four hydrogen bonds (two via oxygen and two via hydrogen) in a tetrahedral configuration. These calculations^{8,27} indicate that at very low temperature, a fifth water molecule tends to joint the first shell of neighbors, favoring a distortion of the tetrahedral configuration in the hydrogen bond network as well as an abundance of dangling-OH bonds. These x-ray studies provide essential information about the bulk, but do not give information about the surface layer of the ice. X-ray techniques adapted to be more sensitive to the surface layer (photon-stimulated desorption–near-edge-x-ray-absorption fine structure) indicate a very slight relaxation of the oxygen-oxygen distance at the surface of ASW.²⁸ Also, the study of the evolution of this distance upon annealing reveals a completely different behavior at surface and in the bulk, showing that the structural evolution within the ice and at the surface can have different histories. Various topological details of the molecular structure, such as the possible existence of pores in the ices, cannot be obtained from the diffraction data. These are, however, of particular importance in the context of gas-surface interaction.

Calculations approximating the ice morphology have been given by Buch and co-workers,^{29–33} who studied amorphous cluster condensation by molecular-dynamics simulation. This model seems to reproduce quite reasonably the local neighborhood of a molecule in bulk H_2O .²⁹ In addition, it provides interesting information concerning the surface molecules: the structure of the $(H_2O)_{450}$ cluster calculated at 10 K presents a highly irregular surface with a large fraction of incompletely coordinated water molecules.³² This picture is supported by IR absorption spectroscopy that has been

shown to be sensitive to the dangling-OH modes of the “surface water molecules”.^{34,35} Experiments involving saturated exposures of H_2 at very low temperatures^{33,36} are consistent with abundant two- and three-coordinated water molecules present at the surface of the ice. In the case of porous ASW, the term surface includes that present within the ice and interacting with the gas.

The study of the desorption kinetics of gases adsorbed on ASW is also a good probe of the gas-surface interaction. Numerous TPD experiments have shown that ASW can adsorb and trap a variety of volatile compounds.^{37–47} The most volatile species (Ar, H_2 , CO, N_2 , O_2 , CH_4) present a main desorption feature at low temperature (< 60 K). Two other features that are independent of the adsorbed species are also present at higher temperature: an abrupt desorption at 140 K corresponding to the onset of crystallization of water (also called “molecular volcano”⁴⁴) and a desorption feature at 160 K corresponding to a codesorption of the gas and water. It has been demonstrated that the gas diffuses into the porous structure of water, and a small part gets trapped by the pores that later collapses upon annealing.^{43,44} This behavior is strongly dependent on the porosity of the ASW film and of the strength of interaction of the molecules with water.

Among the various volatile species studied, molecular hydrogen has the particularity to be the most weakly bound to the water ice surface. Consequently, these molecules diffuse efficiently on the surface, even at very low temperature. Indeed, Rowland *et al.*³⁶ already noted that molecular hydrogen diffuses rapidly into the porous structure of an ASW sample maintained at 10 K, in contrast to N_2 that was found to diffuse above 20 K. In parallel, the H_2 TPD spectra do not show any desorption peak at high temperature (140–160 K).⁴⁵ This behavior is specific to molecular hydrogen because most of the molecules are released before 30 K, that is before the irreversible phase transition of ASW (occurring between 38 and 68 K) responsible for the trapping of the gas. Consequently, the collapse of the porous structure of the film is expected to be limited in a TPD experiment involving molecular hydrogen in the 10–30 K temperature range. Rapid diffusion of hydrogen into the sample at low temperature combined with limited modification of ASW below ~ 30 K make molecular hydrogen a species particularly well suited for probing the highly porous structure of ASW by TPD experiments.

In a recent TPD experiment, Hornekaer *et al.*⁴⁸ have studied the influence of the surface morphology/porosity on the desorption kinetics of D_2 deposited on ASW at 10 K. In this study, the binding energies of the D_2 molecules at the surface of the ice film were measured, revealing an important role of the film thickness in the desorption kinetics. In a parallel investigation, we have observed⁴⁹ a strong isotopic effect in the desorption kinetics of molecular hydrogen after sequential deposition of H_2 and D_2 on 10 K ASW. This effect was explained by considering the competition between H_2 and D_2 for their binding on the same adsorption sites.

In the present study, we focus on the D_2 desorption kinetics on a 10 ML ASW film grown at 10 K by background deposition. The D_2 dose dependency is particularly investigated, in complement to previous investigation.⁵⁰ Exposures

ranging from very low coverage up to the saturation coverage on the film maintained at 10 K are used. The dose dependency is then carefully analyzed in order to determine the binding energies of D₂ physisorbed on the porous surface of the ASW film. We first use the Arrhenius plot method for that purpose. Due to the large uncertainties provided by this method, we next propose a simple model describing the interaction of molecular hydrogen (D₂) with ASW at any temperature. We show that this approach can provide an interesting tool for recovering the binding-energy distributions at any coverage. The results are revealing the highly heterogeneous character of ASW.

II. EXPERIMENT

The recently commissioned formation of molecules in the interstellar medium (FORMOLISM) experimental setup has been developed for the purpose of studying the reaction processes of atoms and molecules on surfaces that mimic grains under conditions relevant to astrophysics. The extensive capabilities of the experiment and a complete description of the setup will be presented in a forthcoming paper.⁵¹ The parts of the system that are used in this study are briefly described below. The experiments are performed in an ultrahigh-vacuum chamber with a base pressure of less than 10⁻¹⁰ mbar. The sample holder consists of an oxygen-free high conductivity (OFHC) copper cylinder block in good thermal contact with the cold finger of a He closed cycle cryostat (ARS Displex DE-204S) equipped with an 800 K heating interface. The temperature is measured using a calibrated silicon diode and a thermocouple (AuFe/Chromel) clamped on the sample holder, both connected to a temperature controller (Lakeshore 340). The temperature was calibrated by monitoring the multilayer desorption of CO and Ar from the sample surface.⁵² The temperature can be controlled to ±0.2 K and measured with an accuracy of ±1 K. The de-ionized water samples have previously undergone several outgassing cycles.

In the present investigation, the H₂O ice films were grown in two steps as follows. At first, a microchannel array doser (1 cm in diameter) was installed at 2 cm in front of the copper surface (1 cm in diameter) maintained at 120 K. This layout was used to grow about 150 ML of nonporous ice. [Although the term “bilayer” (BL) is widely used to describe a complete single water layer, the unit used throughout this paper is defined as follows: 1 ML = 10¹⁵ cm⁻².] In the second step, the water vapor is introduced into the vacuum chamber through a leak valve (“background” deposition) after cooling the surface down to 10 K. By using this technique, an outer layer of highly porous water ice is grown at a rate of 0.006 ML/s. The amount of water deposited corresponds to 10 ML, assuming the sticking coefficient of water at 10 K to be unity. The first layer of nonporous ice is used to isolate the porous film from the metallic substrate, in order to avoid complications in the TPD spectra arising from the interaction of the gas with the underlying hydrophilic substrate.⁵³

In a typical experiment the ice film is exposed for a given amount of time to D₂, which is also introduced by background deposition, while the sample temperature is

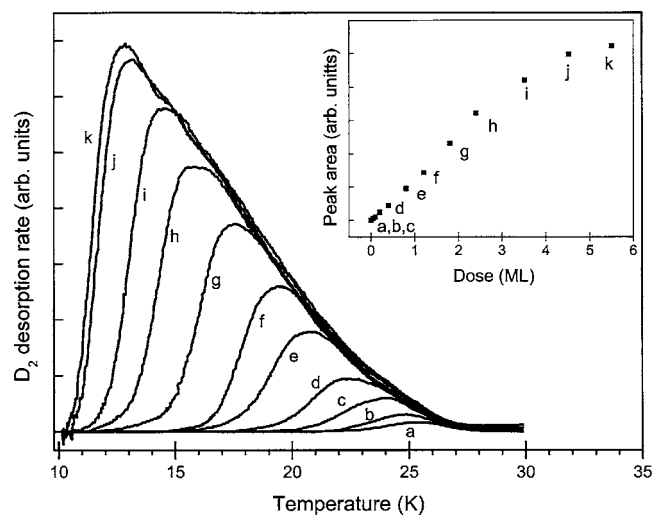


FIG. 1. TPD spectra for increasing D₂ doses on a 10 ML porous ASW film grown at 10 K. The inset shows the integrated signal as function of dose. 1 ML = 10¹⁵ molecules/cm². (a) 0.05 ML, (b) 0.1 ML, (c) 0.2 ML, (d) 0.4 ML, (e) 0.8 ML, (f) 1.2 ML, (g) 1.8 ML, (h) 2.4 ML, (i) 3.5 ML, (j) 4.5 ML, and (k) 5.5 ML.

maintained at 10 K. The incoming gas is composed of a normal mixture of ortho-D₂ and para-D₂ at 300 K. A quadrupole mass spectrometer (QMS, HIDDEN 3F/PIC), that can be rotated and translated, is then placed at 3 mm in front of the sample for the purpose of TPD experiments. A linear temperature ramp at a rate of 0.17 K/s is used. In order to ensure that the first and subsequent measurements are made on a sample with the same thermal history, a blank experiment (without introduction of D₂) is performed before the first D₂ TPD experiment. Due to the open geometry of our QMS head, it is also impossible to avoid contributions from other parts of the cooling system. Therefore, for each of the spectra, a second D₂ TPD experiment is systematically made with the QMS 130 mm away from the sample. This signal is subsequently subtracted from that obtained with the QMS placed in front of the sample.

III. RESULTS AND DISCUSSION

A. Experimental results

Figure 1 shows a series of D₂ TPD spectra obtained on an ~10 ML porous ASW film. As explained in the above section, the ice film was grown at 10 K by background deposition over a 150 ML nonporous ice base previously grown at 120 K. In these conditions, the porous layer is completely isolated from the copper substrate. The sequence of TPD spectra shown in Fig. 1 has been recorded for increasing [from (a) to (k)] initial D₂ exposures. We have checked that the TPD spectra are reproducible and not dependent on the order of the dose sequence. At the lowest exposures, the desorption rate is maximum around 25 K. At higher exposures, the maximum of desorption increases and shifts progressively towards 15 K, while the curves broaden towards lower temperatures. The way these curves overlay their trailing edges and progressively peak at lower temperatures is very similar to what Kimmel *et al.*¹⁸ have observed in the 25–45 K temperature range for N₂. As explained by these

authors, this behavior characterizes several important properties of the gas-surface interaction. For the spectra recorded after low exposures, the gas is released at high temperatures, showing that the molecules tend to be more tightly bound to the surface at low coverages. This implies that the molecules are mobile enough to explore the surface and find the strongest bonding sites prior to desorption. Figure 1 shows that new adsorption sites corresponding to lower desorption temperatures (and therefore to lower binding energies) are progressively filled as the doses increase. Finally, the extended range of desorption temperatures is the signature of a wide range of binding energies available on the surface. The origin of such a wide energy distribution is linked to the disordered nature of the water ice surface. As noted in the Introduction, the surface to be considered in the case of our porous film is not restricted to the external part of the film, but includes additional adsorption sites located within the film. The complex geometry of the ice film, that can possibly contain tunnels and pores of different sizes, leads to a large variety of adsorption sites associated to various interactions with D_2 . The interaction of the molecules with the surface is also known to differ significantly between ortho and para species due to difference in the symmetry of their rotational wave function, respectively.⁵⁴ In this study, the ice film has been exposed to molecular gas at room temperature which is composed of a statistic mixture of ortho- D_2 and para- D_2 that have distinct binding energies with the ice surface. In addition, interactions between adjacent D_2 molecules might contribute to the energy dispersion, in particular, because their relative distance cannot be reduced as compared to the same density of molecules distributed over a flat surface.

The inset in Fig. 1 shows the integrated TPD intensities as a function of the exposed D_2 doses. The doses quoted are determined by calculating the number of molecules hitting a unit surface considering both the D_2 background pressure and the exposure time. Doses are given in equivalent monolayer unit (1 ML = 10^{15} cm⁻²). Figure 1 indicates that the sticking coefficient is constant up to 3 ML and decreases above this limit. For a sample temperature of 10 K, a saturation is achieved around 4.5 ML (curve j in Fig. 1). Higher doses do not cause any evolution in the TPD spectra, as shown on curves j and k in Fig. 1. These spectra show a very abrupt start, indicating that the molecules are escaping from the surface almost simultaneously with the beginning of the heating process. In other words, the tentative addition of more D_2 molecules on the 10 K surface leads to their desorption at a rate equal to their adsorption rate. This saturation behavior does not imply, however, that the ice surface has been actually fully covered. Indeed, no signature of D_2 desorption arising from multilayers can be identified on the TPD spectra (Fig. 1). Hornekaer *et al.*⁵⁰ have assigned a D_2 bilayer desorption peak to a TPD feature arising at 9 K in an experiment concerning a nonporous ASW film. The same kind of signature could be expected at higher temperature in the case of a porous ASW film.¹⁸ Moreover, the D_2 multilayer desorption is known to peak at 7 K.⁵² In our experiment, the sample temperature (10 K) is high enough to prevent the formation of any type of multilayers. We con-

clude that the saturation dose obtained in this study conducted at 10 K is below but very close to a full coverage of the ice surface.

We point out that the doses quoted in Fig. 1 are related to the number of molecules/cm² impinging on the surface. The number of molecules actually present on the sample at $T = 10$ K is a proportion of the previous number, due to the sticking probability. Adopting a sticking probability of $\sim 0.6-1$ for porous ice,⁵⁰ the effective density of molecules present at saturation coverage on the 10 K surface is about $N = 2.7-4.5$ ML. Another important parameter, the porosity, can be estimated from the saturation coverage. The porosity ξ is defined as the fraction of internal surface area, relative to the external surface area per monolayer of ASW: $\xi = (N-1)/N_{ASW}$, where N_{ASW} is the thickness of the ice sample expressed in monolayer and where the external surface area considered is 1 ML. Using $N_{ASW} = 10$ ML, ξ is estimated between 0.17 and 0.35.

The minimum dose (0.05 ML) used in our experiment is 1% of that required for the saturation of the film at 10 K. Thus, our series of D_2 TPD spectra spans a very extended set of coverages (1% to $\sim 100\%$) that provide a wide base for the determination of the coverage dependence of the D_2 binding energies on the surface of ASW, as described in the following sections.

B. Analysis of the experimental data

Several procedures are currently used in surface science and catalysis in order to analyze the TPD experiments. Thermal desorption is usually described in terms of an Arrhenius expression as

$$R(\theta) = -d\theta/dt = A(\theta)\theta^n \exp[-E(\theta)/kT], \quad (1)$$

where R is the desorption rate, θ the adsorbate coverage, t the time, A the preexponential factor of desorption, n the order of the desorption process, k the Boltzmann constant, T the temperature, and E the activation energy for desorption. The temperature T and the time t are related by $dT/dt = \beta$, where β is the heating rate. Several approximations, such as assuming a θ -independent preexponential factor, are frequently made in order to simplify Eq. (1). In this way, the analysis of the TPD signal $S(T)$ can be applied to a single spectrum. In the present study, we use Eq. (1) without any further assumption than considering a first-order desorption, which applies here because desorption occurs at submonolayer coverage, as established in the above section. The series of desorption spectra corresponding to different initial coverages permits the so-called *complete analysis*⁵⁵ to be applied. The coverage is defined here with respect to the saturation dose, i.e., $\theta(T)$ is the ratio of the area of a TPD spectrum for temperatures ranging above T , by the total area of the saturated TPD curve, $\theta(T) = \int_T^\infty S_x(T')dT' / \int_0^\infty S_j(T')dT'$ where $S_j(T)$ is related to the curve j in Fig. 1 and $x = a, b, c$, etc. Thus, desorption rates $R_\theta(T)$ corresponding to a given coverage θ are determined on the different available spectra. An Arrhenius plot of $\ln(R_\theta)$ vs $1/T$ yields $E(\theta)$, while the origin intercept provides $\ln[A(\theta)]$. Figure 2 displays the binding energies and the preexponential factors A derived

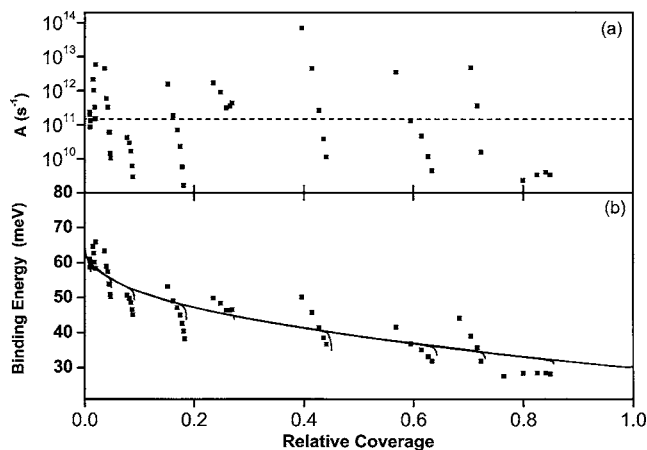


FIG. 2. The set of couples (preexponential factor A , energy E) given by the complete analysis. (a) A values associated with the energies E shown in (b). The full line is the constant A value that minimizes the absolute minimum deviation: $A \sim 10^{11} \text{ s}^{-1}$. (b) Binding energies E plotted for various selected coverages. The full lines are obtained from Eq. (1) with $A=10^{11} \text{ s}^{-1}$ for the curves a–j shown in Fig. 1. The coverage is defined with reference to the saturation coverage at 10 K (see text).

from this method for a set of coverages. In order to illustrate the precision obtained by this method, we have repeated this procedure a few times for small variations of the coverages. This results in a cloud of points, as shown in Fig. 2. Despite the high dispersion of the results, we observe a strong correlation between the values of the preexponential factor $A(\theta)$ [Fig. 2(a)] and the values of the energies $E(\theta)$ [Fig. 2(b)]. The highest values for the preexponential factors are correlated with the highest energies and conversely. Facing the difficulty of finding a significant variation of A with coverage, we therefore choose to use a constant preexponential factor $A=10^{11} \text{ s}^{-1}$ that corresponds to the absolute minimum deviation.

Once the value of A has been set to a constant, the energies $E(\theta)$ can be obtained by direct inversion of Eq. (1) as follows: $E(\theta) = -kT \ln[-R/A\theta]$. The results of such inversion applied to each of our TPD spectra (Fig. 1), using for $A=10^{11} \text{ s}^{-1}$, are represented by the full lines shown in Fig. 2(b). The curves $E(\theta)$ corresponding to different TPD curves (and therefore to different initial coverages) pass roughly through the same values. The same quality of superposition between these curves has also been obtained for $A=10^{11 \pm 2} \text{ s}^{-1}$, confirming the difficulty to constrain this value.

The population distribution $P(E)$ of the molecules over the binding sites with binding energy E can also be obtained. Writing the coverage in all adsorption sites of binding energy larger than E as $\theta(E) = \int_E^\infty P(E) dE$, $P(E)$ can be computed as $P(E) = -d\theta/dE$. The distribution $P(E)$ derived from Fig. 2(b) are plotted in Fig. 3.

In the case of first-order desorption, A corresponds to the vibrational frequency ν_0 of the molecules at the surface, and is typically considered to lie between 10^{12} and 10^{13} s^{-1} . We should keep in mind at this stage of the analysis that the desorption rates may be affected by the structure of a porous sample. As previously pointed out by Hornekaer *et al.*,⁵⁰ the molecules adsorbed at the top of the sample are more easily released in the gas phase than those lying inside the film that

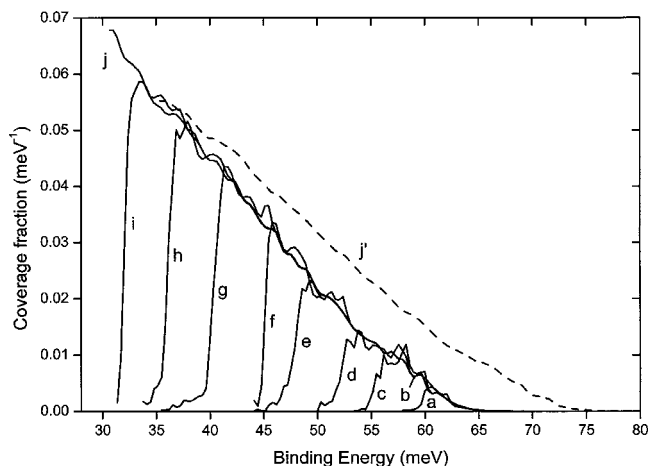


FIG. 3. The D₂ population $P(E)$ vs binding energy derived from a direct inversion of the D₂ TPD spectra obtained on a 10 ML porous ASW film. The letters refer to the spectra shown in Fig. 1. A constant preexponential factor is used. (a–j) $A=10^{11} \text{ s}^{-1}$; (j') $A=10^{13} \text{ s}^{-1}$.

are more likely to be readsorbed on the walls of tunnels, cavities, or pores. Consequently, molecules that actually contribute to the instantaneous desorption rates are only a fraction ε of those lying on the top of the film surface. Following these authors and assuming a uniform D₂ distribution throughout the film, Eq. (1) should be rewritten as follows: $R(\theta) = (\varepsilon\nu_0)\theta \exp[-E(\theta)/kT]$. Consequently, the complete analysis leads to the determination of an apparent preexponential factor $A = \varepsilon\nu_0 < \nu_0$. According to the estimations made in the previous section concerning the porosity ξ , this effect could account for a maximum lowering of A by a factor $(1 + N_{\text{ASW}}\xi) \approx 4$, as compared to ν_0 . The small impact of this effect is due to the use of a very thin sample in our experiment ($N_{\text{ASW}}=10 \text{ ML}$).

This complete analysis method finally does not allow to constrain confidently the preexponential factor within less than few orders of magnitudes. Since A and E are correlated, it is important to consider the impact of such a large uncertainty for A on the binding-energy determination. For this reason, we have also computed the population distribution $P(E)$ for $A=10^{13} \text{ s}^{-1}$. Figure 3 shows that a variation of A by two orders of magnitude causes the population distribution to be shifted by about 10 meV towards higher energies. Figure 3 clearly shows that the high binding-energy population is coverage independent, while the lowest binding-energy population is on the contrary strongly coverage dependent. As already seen on the TPD spectra that exhibit very similar profiles, this behavior is the signature of a sequential filling of binding sites, from the most to less energetic ones.

Hornekaer *et al.*⁵⁰ have determined the binding energies from a 1.2 ML D₂ dose on a 20 ML porous ($\xi \sim 0.1$) ASW sample. They found energies ranging between 40 and 60 meV. Our curve f in Fig. 3, that corresponds to the same D₂ dose, covers the 45–65 meV energy range, which is in very good agreement. However, the profiles of the distributions $P(E)$ are different. The population distributions found in the present study are very wide and asymmetric. They peak at the lowest available binding energies, reflecting the general shapes of the TPD spectra. The TPD experiments

made after thermal annealing of porous ASW films suggest that the high binding energies should correlate to binding sites located within the ice film,⁵⁰ while the lowest energies are more concerned by the external surface of the film. The profile of these distributions are therefore directly governed by the morphology of the film and by the number and the nature of the binding sites found by the molecules within the ice structure of the film. Moreover, Kimmel *et al.*¹⁸ have shown that at small thickness (less than 25 ML), the pore structure of ASW is not fully developed. As a result, the general profile of the binding-energy distribution should be particularly sensitive to the ice thickness in the case of thin films.

Our study clearly shows an important property of the D₂-ASW interaction: the binding energy of molecular hydrogen on a porous ASW sample is highly dose dependent and can vary by a factor of 2 with coverage. We point out that such behavior should be taken into account in experiments, or calculations, involving various doses of molecular hydrogen adsorbed on a porous ASW sample. We add that the energy variation induced by the coverage exceeds by far the small differences observed in the binding energies of the various molecular hydrogen isotopes⁴⁹ (principally H₂ and D₂). This property is also in line with molecular-beam experiments conducted on polycrystalline water ice at very low temperature,^{56,57} that have also shown a coverage dependency for the binding energies.

In conclusion, the method used in the present section to derive the binding energies appears to be dependent on the preexponential factor. This factor is not very well constrained by extrapolation to the origin of the Arrhenius plot. We have also noted that this method is not very well suited to the TPD spectra obtained in this study. Indeed, we have seen that due to the sequential filling behavior of the adsorption sites, the spectra overlap in the high-temperature range. In these common parts of the spectra, the desorption rates are about the same at the same coverage. Thus, they are not useful in an Arrhenius plot analysis. Consequently, only a very few points located at the leading edge of the TPD spectra can be actually used for the Arrhenius plot. Unfortunately, these points are close in temperature, making this method difficult to apply confidently. In the next section, we adopt a new approach that allows the fitting of the experimental results and leads in addition to an easy description of the binding-energy distribution of the molecules at any coverage.

C. Model of experimental data

We propose here a simple model in order to describe the binding energies of molecular hydrogen interacting with ASW, at any coverage and any temperature. One has first to note the high mobility of molecular hydrogen, which can be estimated by considering the competition between desorption and diffusion, as shown by Kimmel *et al.*¹⁸ in the case of N₂. The average desorption and diffusion lifetimes are given by $\tau_{\text{des}} = C e^{E_d/kT}$ and $\tau_{\text{diff}} = D e^{E_d/kT}$, respectively, C and D being constants. The energy barrier for diffusion E_d is generally a fraction of the binding energy E_a . Assuming $C \sim D$ and adopting $E_d = E_a/3$, we can estimate the number of steps

prior to desorption as $N = e^{2E_d/3kT}$. At $T = 10$ K and considering the lowest binding energies ($E_a \sim 30$ meV), the number of steps is $N = 10^9$. This is about the same for the highest binding energies ($E_a \sim 65$ meV) that are only involved when the temperature has increased (that is typically $T = 25$ K). Even if a barrier for diffusion as high as $3/4 E_a$ is adopted, the number of steps remains as large as 3×10^3 at $T = 10$ K. We conclude that at any step of the heating process, the molecule can explore a huge variety of adsorption sites available on the ASW surface, prior to desorption. Consequently, we propose to describe the population distribution by assuming the molecules to be continuously in complete thermal equilibrium with the surface. We also assume the molecules to explore the overall available adsorption sites. Although diffusion is not actually the same for all the molecules, we will see that only those having large mobility are concerned by a statistical redistribution with temperature. Due to the sequential filling of the adsorption sites (as already explained above), the function $g(E)$ describing the distribution of adsorption sites has to recover population distribution found by direct inversion. Based on the shape of the distribution found for the highest dose (curve j in Fig. 3) in the previous section, we adopt a polynomial function $g(E) = a(E_0 - E)^b$, where a , E_0 , and b are parameters to be determined from the TPD analysis. This distribution has to be populated taking into account that one molecule only is allowed per adsorption site. With such an exclusion constraint, the appropriate statistical law is the Fermi-Dirac distribution function. At a given temperature T , the population of molecules $P(E)$ distributed over a set of available sites $g(E)$ is thus given by

$$P(E, T, \mu) = g(E) \left\{ 1 + \exp\left(-\frac{(E - \mu)}{kT}\right) \right\}^{-1}, \quad (2)$$

where μ is the chemical potential, which can be obtained by the closing relation,

$$\int P(E, T, \mu) dE = \theta(T).$$

In a second step of the calculations, we simulate the heating of the sample. Thus, starting with saturation coverage, we calculate the initial population distribution at $T = 10$ K. We then compute, following Eq. (1), the variation of coverage due to a small increase in temperature (ΔT). At each temperature step, the population is redistributed following Eq. (2) and a new μ parameter is determined. The procedure enables a simulation of the whole set of experimental TPD curves presented in Fig. 1. By using a least-squares fitting approach (Levenberg-Marquardt nonlinear fitting procedure), we have adjusted the parameters defining the curve $g(E)$ as well as the preexponential factor describing the desorption. The parameters found using this approach are the following: $E_0 = 78.9$ meV, $a = 1.23 \times 10^{-4}$, $b = 1.6$, and $A = 10^{13} \text{ s}^{-1}$. The excellent agreement between the simulated and experimental TPD curves is illustrated in Fig. 4. The inset in Fig. 4 displays the adjustment of the preexponential factor. In comparison with the previous determination made by direct inversion, we note that both results are consistent but that higher values of the preexponential factor are favored by the

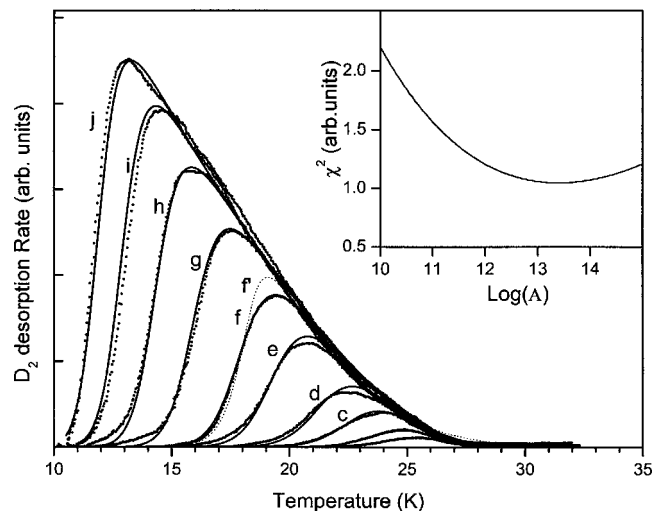


FIG. 4. Experimental (points) and simulated (full lines) and TPD curves for increasing D₂ doses on a 10 ML ASW film. The experimental doses are given in Fig. 1 caption. *f'* same as *f* but without allowing redistribution of the population (see text). The inset shows the least-square fitting for the preexponential *A*.

fitting procedure, $A \sim 10^{13} \text{ s}^{-1}$, giving the best fit, as shown in the inset of Fig. 4. Due to the direct correlation between *A* and *E* (discussed above), this tends to reinforce the tail of the population distributions for the highest binding energies. The optimized population distribution $g(E)$ is plotted in Fig. 5. This distribution reaches even slightly higher energies ($\sim 80 \text{ meV}$) than, those found by direct inversion with $A = 10^{13} \text{ s}^{-1}$ ($\sim 75 \text{ meV}$ in Fig. 3).

The paramount importance of the mobility in this approach has been tested. This is illustrated by curve *f'* in Fig. 4, which has been obtained with the same initial coverage as for curve *f*, but without any redistribution of the molecules with temperature. The molecules were identically initially distributed over their adsorption sites at 10 K in both cases. Obviously, the curve *f'* cannot reproduce the experimental

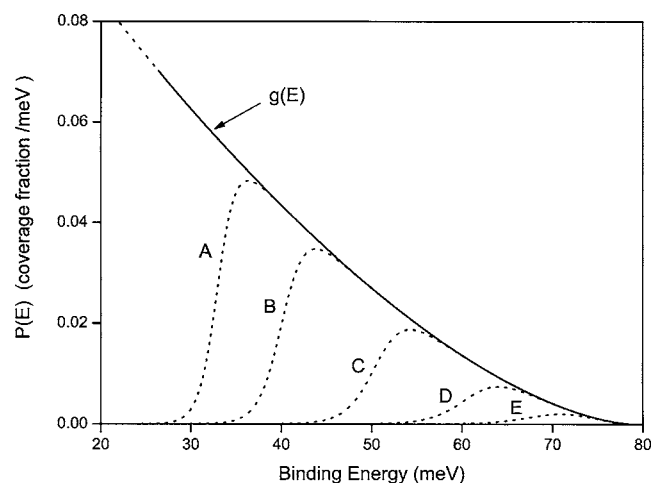


FIG. 5. Model for desorption kinetics. The full line represents the binding-energy distribution for adsorption sites available on the surface of the sample. The dotted lines show the evolution of the D₂ binding-energy distribution at several temperatures during the heating process. (A) $T=10 \text{ K}$ with maximum coverage, (B) $T=15 \text{ K}$, (C) $T=18.5 \text{ K}$, (D) $T=22 \text{ K}$, and (E) $T=25 \text{ K}$.

spectrum (Fig. 4). This demonstrates the crucial role of a continuous redistribution of the molecules with temperature during the heating process. This also indirectly supports evidence for the high mobility of the molecules.

Figure 5 shows the binding-energy distributions obtained by Eq. (2) for five selected temperatures. It provides snapshots of the population distribution $P(E)$ at different steps of the heating process. The distributions show that the most energetic adsorption sites are always completely occupied. The Fermi-Dirac statistics only affects the manner in which molecules distribute over less energetic sites, that are precisely those diffusing very fast, supporting the initial assumption concerning the thermal equilibrium. Curve A shows the initial distribution before the start of the heating process ($T=10 \text{ K}$), and for maximum coverage. Curve E is obtained at $T=25 \text{ K}$ when most of the molecules have already been released in the gas phase. The profiles are very asymmetric at high coverage and tend to be more symmetric at low coverage (from curves A to E). This characterizes an evolution in the filling of the adsorption sites. One can note, in particular, that the molecules tend to spread over a wide variety of binding sites at very low coverages and do not accumulate in the most energetic ones. This peculiar behavior cannot be obtained from a direct inversion of the TPD profiles. Indeed, this view of the energy distribution is markedly different from that given by the direct inversion. The distributions shown in Fig. 5 are indeed not equivalent to those presented in Fig. 3, although both can be used to reproduce the same desorption curves. Those determined by direct inversion of the TPD curves (Fig. 3) result from the overall dynamic heating process. They provide the evolution of population during the TPD experiment. Those defined in the model (Fig. 5) are adjusted to represent a finite population of molecules at fixed temperature, in the hypothesis of a complete thermal equilibrium and statistical filling of adsorption sites. One of the main interests of this simulation approach is thus to provide a view of the population distributions at any temperature, independently of the dynamical heating process.

Another interesting application of this approach is the possibility to describe the competition between different species that are susceptible to fill the same adsorption sites. We have indeed successfully used the same type of model to describe dramatic differences observed in the TPD experiments involving H₂ and D₂ mixtures.⁴⁹ In the model, the same distribution $g(E)$ was used for the two species H₂ and D₂ except that the zero-point binding-energy difference is taken into account. The presence of the other isotope also has to be included since it changes the number of available adsorption sites. Different population distributions $P(E)$ are found for H₂ and D₂, respectively. The most energetic sites are found to be preferentially filled by D₂, in good agreement with the experiment.

D. Comparison with H₂O clusters results

Fourier-transform infrared (FT-IR) spectroscopic studies and calculations of the surface ice-adsorbate interactions of various volatiles have been based on the assignment of spe-

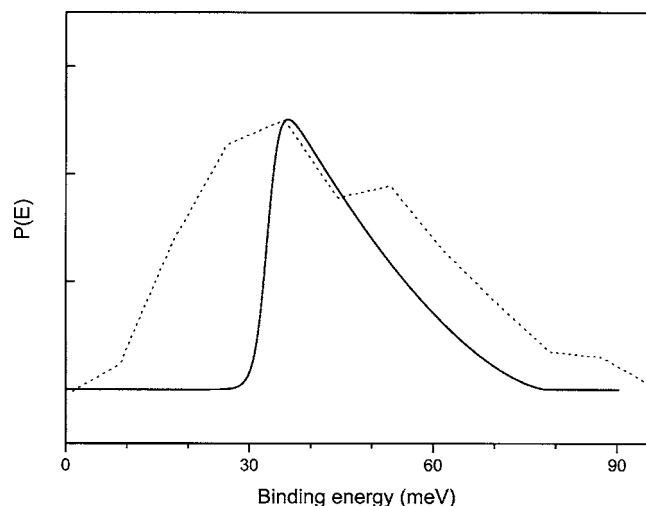


FIG. 6. Solid line: simulated binding-energy distribution given by the model for maximum coverage at $T=10$ K (this study). Dotted line: binding-energy distribution obtained after zero-point energy shifting of the calculated potential minima for molecular hydrogen interacting with water clusters (Ref. 33). The vibrational frequency has been set to 10^{13} s $^{-1}$.

cific adsorption sites, such as three-coordinated water molecules with either a dangling-H or a dangling-O coordination and four-coordinated water molecules with coordination shells distorted with respect to tetrahedral symmetry.^{58,59} The wide and continuous energy distributions obtained in the present study suggest a very wide variety of adsorption sites. Indeed, computation modeling of amorphous ice as described by large H₂O clusters does show a wide and continuous range of the potential minima.³³ The features of the H₂O cluster used in such models include a broad distribution of angles between adjacent water molecules, a broad distribution of bond coordination of water molecules, and an abundance of “dangling atoms.” In addition, various geometric configurations of molecular hydrogen with respect to the water molecules, associated with different numbers of water molecules interacting with D₂,⁵⁰ contribute to the spreading of the adsorption energy minima. In order to compare our experimental results with this model of H₂O cluster, the calculated distribution of energy minima³³ has been shifted by $h\nu_0/2$ (zero-point energy), using $\nu_0=10^{13}$ s $^{-1}$, as determined by the fitting procedure described above in Sec. III C. In Fig. 6, this distribution is compared to that obtained by our model for maximum coverage at $T=10$ K. The very good agreement between both distributions in their common energy range is very satisfying. It should be mentioned that such consistency is obtained when using vibrational frequencies close to 10^{13} s $^{-1}$, whereas lower values would give calculated energies significantly higher than those derived from the experiment. The striking similarity in the shape of both energy distributions is an indication of similar and strong heterogeneity for the surface water cluster as for the thin and porous ASW film used in this study. If this is correct, the calculation also predicts the existence of adsorption sites with even lower binding energy that could not be probed in the experiment.

IV. CONCLUSION

We have presented a set of TPD experiments that allows studying in detail the interaction of D₂ with a porous and thin (~ 10 ML) ASW film. The results open new insights into the characterization of the binding-energy distribution of the molecules adsorbed on ASW, and point out the peculiar high coverage dependency of these distributions. Molecular hydrogen that diffuses into the porous structure of the ice is considered here as an ideal probe of the gas-surface interaction, in a temperature range where the modification of the ice structure induced by thermal annealing should be rather limited. We have investigated the desorption kinetics at successive increasing D₂ dose, ranging from very low coverage up to the saturation of the film maintained at 10 K. This systematic approach enables a *complete analysis* method, which does not require any assumption concerning the value of the preexponential factor of the Arrhenius expression, and which provides the binding energies. This analysis leads to the determination of a wide and continuous distribution of the binding energies, presenting a maximum of population peaking at low energy for all the coverages probed in this experiment. We have further fitted a unique set of binding-energy distributions for the adsorption sites, by using a simple model describing the progressive filling of the adsorption sites at any temperature. The model assumes a thermal equilibrium of the molecules with the surface, even during the heating process. This approach leads to a very satisfying simulation of the TPD experiments and gives a very simple description of the population distribution at any coverage and any temperature. This approach also shows how the binding-energy distribution evolves during the heating process, revealing the natural tendency of the molecules to fill a large subset of binding energies, even at very low coverage.

The existence of such a wide range of binding energies could have interesting consequences in the astrophysical context, because the strength of the binding energy is closely related to the residence time of a molecule on a given site. For a typical water ice grain mantle at 10 K, as found in dark clouds, the average residence time of molecular hydrogen can indeed vary from 100 days up to 10^9 years depending upon the actual coverage of the grain mantles. An application of this model could be the calculation of the number density of molecular hydrogen that would accumulate at the surface of icy grain mantles, in physical conditions relevant for dark clouds, including, for example, lower temperatures than those used in the present experiment.

In conclusion, we believe that systematic TPD experiments using different types (porous, less porous, nonporous, and crystalline) water ices are necessary in order to compare in detail the energy distribution of their adsorption sites. The use of molecular hydrogen as a probe of the ice structure at low temperature in combination with the TPD technique seems to be well suited. The model presented here might help for this purpose and can serve as a template for future studies. These investigations are under progress in our laboratory.

ACKNOWLEDGMENTS

The authors thank Dr. F. Rostas for careful reading of the manuscript and for useful suggestions. The authors acknowledge support of the national PCMI program funded by the CNRS, as well as the strong financial support from the Conseil Régional d'Ile-de-France (SESAME program E1315) and the Conseil Général du Val d'Oise.

- ¹R. S. Smith and B. D. Kay, *Nature* (London) **398**, 788 (1999).
- ²R. S. Smith, C. Huang, and B. D. Kay, *J. Phys. Chem. B* **101**, 6123 (1997).
- ³P. Ehrenfreund, H. J. Fraser, J. Blum, J. H. E. Cartwright, J. M. Garcia-Ruiz, E. Hadamcik, A. C. Levasseur-Regourd, S. Price, F. Prodi, and A. Sarkissian, *Planet. Space Sci.* **51**, 473 (2003).
- ⁴L. J. Almandola, S. A. Bernstein, and R. L. Walker, *Space Sci. Rev.* **90**, 219 (1999).
- ⁵P. Ehrenfreund and S. B. Charnley, *Annu. Rev. Astron. Astrophys.* **38**, 427 (2000).
- ⁶E. L. Gibb, D. C. B. Whittet, W. A. Schutte *et al.*, *Astrophys. J.* **536**, 347 (2000).
- ⁷P. Ehrenfreund and W. A. Schutte, *Adv. Space Res.* **25**, 2177 (2000).
- ⁸P. Jenniskens, D. F. Blake, M. A. Wilson, and A. Pohorille, *Astrophys. J.* **455**, 389 (1995).
- ⁹A. Kouchi, T. Yamamoto, T. Kozasa, T. Kuroda, and J. M. Greenberg, *Astron. Astrophys.* **290**, 1009 (1994).
- ¹⁰W. Hagen, A. G. G. M. Tielens, and J. M. Greenberg, *Chem. Phys.* **56**, 367 (1981).
- ¹¹M. E. Palumbo, *J. Phys. Conf. Ser.* **6**, 211 (2005).
- ¹²E. Mayer and R. Pletzer, *Nature* (London) **319**, 298 (1986).
- ¹³R. Pletzer and E. Mayer, *J. Chem. Phys.* **90**, 5207 (1989).
- ¹⁴C. Martin, C. Manca, and P. Roubin, *Surf. Sci.* **502–503**, 280 (2002).
- ¹⁵C. Martin, C. Manca, and P. Roubin, *Surf. Sci.* **502–503**, 275 (2002).
- ¹⁶M. S. Westley, G. A. Baratta, and R. A. Baragiola, *J. Chem. Phys.* **108**, 3321 (1998).
- ¹⁷K. P. Stevenson, G. A. Kimmel, Z. Dohnálek, R. S. Smith, and B. D. Kay, *Science* **283**, 1505 (2001).
- ¹⁸G. A. Kimmel, K. P. Stevenson, Z. Dohnálek, R. S. Smith, and B. D. Kay, *J. Chem. Phys.* **114**, 5284 (2001).
- ¹⁹Z. Dohnálek, G. A. Kimmel, P. Ayotte, R. S. Smith, and B. D. Kay, *J. Chem. Phys.* **118**, 364 (2003).
- ²⁰G. A. Kimmel, Z. Dohnálek, K. P. Stevenson, R. S. Smith, and B. D. Kay, *J. Chem. Phys.* **114**, 5295 (2003).
- ²¹D. E. Brown, S. M. George, C. Huang, E. K. L. Wong, K. B. Rider, R. S. Smith, and B. D. Kay, *J. Phys. Chem.* **100**, 4988 (1996).
- ²²A. H. Narten, C. G. Venkatesh, and S. A. Rice, *J. Chem. Phys.* **64**, 1106 (1976).
- ²³P. Jenniskens and D. F. Blake, *Science* **265**, 753 (1994).
- ²⁴B. Guillot and Y. Guissani, *J. Chem. Phys.* **119**, 11740 (2003).
- ²⁵B. Guillot and Y. Guissani, *J. Chem. Phys.* **120**, 4366 (2004).
- ²⁶A. Bizid, L. Bosio, A. Defrain, and M. Oumezzine, *J. Chem. Phys.* **87**, 2225 (1987).
- ²⁷B. Guillot and Y. Guissani, *J. Chem. Phys.* **120**, 4366 (2004).
- ²⁸Ph. Parent, C. Laffon, C. Mangeney, F. Bournel, and M. Tronc, *J. Chem. Phys.* **117**, 10542 (2002).
- ²⁹Q. Zhang and V. Buch, *J. Chem. Phys.* **92**, 5004 (1990).
- ³⁰Q. Zhang and V. Buch, *J. Chem. Phys.* **92**, 1512 (1990).
- ³¹V. Buch, *J. Chem. Phys.* **93**, 2631 (1990).
- ³²V. Buch, *J. Chem. Phys.* **96**, 3814 (1992).
- ³³H. G. Hixson, M. J. Wojcik, M. S. Devlin, J. P. Devlin, and V. Buch, *J. Chem. Phys.* **92**, 753 (1992).
- ³⁴V. Buch and J. P. Devlin, *J. Chem. Phys.* **94**, 4091 (1991).
- ³⁵J. P. Devlin and V. Buch, *J. Phys. Chem.* **99**, 16534 (1995).
- ³⁶B. Rowland, M. Fisher, and J. P. Devlin, *J. Chem. Phys.* **95**, 1378 (1991).
- ³⁷A. Bar-Num, G. Herman, D. Laufer, and M. L. Rappaport, *Icarus* **63**, 317 (1985).
- ³⁸A. Bar-Num, J. Dror, E. Kovhavi, and D. Laufer, *Phys. Rev. B* **35**, 2427 (1987).
- ³⁹D. Laufer, E. Kochavi, and A. Bar-Num, *Phys. Rev. B* **36**, 9219 (1987).
- ⁴⁰G. Natesco and A. Bar-Num, *Icarus* **126**, 336 (1997).
- ⁴¹M. P. Collings, J. W. Dever, H. J. Fraser, and M. R. S. McCoustra, *Astrophys. Space Sci.* **285**, 633 (2003).
- ⁴²M. P. Collings, M. A. Anderson, R. Chen, J. W. Dever, S. Viti, D. A. Williams, and M. R. S. McCoustra, *Mon. Not. R. Astron. Soc.* **354**, 1133 (2004).
- ⁴³M. P. Collings, J. W. Dever, H. J. Fraser, M. R. S. McCoustra, and D. A. Williams, *Astrophys. J.* **583**, 1058 (2003).
- ⁴⁴R. S. Smith, C. Huang, E. K. L. Wong, and B. D. Kay, *Phys. Rev. Lett.* **79**, 909 (1997).
- ⁴⁵R. W. Dissly, M. Allen, and V. G. Anicich, *Astrophys. J.* **435**, 685 (1994).
- ⁴⁶R. L. Hudson and B. Donn, *Icarus* **94**, 326 (1991).
- ⁴⁷A. Bar-Num, I. Kleinfeld, and E. Kochavi, *Phys. Rev. B* **38**, 7749 (1988).
- ⁴⁸L. Hornekaer, A. Baurichter, V. V. Petrunin, D. Field, and A. C. Luntz, *Science* **302**, 1943 (2003).
- ⁴⁹F. Dulieu, L. Amiaud, S. Baouche, A. Momeni, J.-H. Fillion, and J.-I. Lemaire, *Chem. Phys. Lett.* **404**, 187 (2005).
- ⁵⁰L. Hornekaer, A. Baurichter, V. V. Petrunin, A. C. Luntz, B. D. Kay, and A. Al-Halabi, *J. Chem. Phys.* **122**, 124701 (2005).
- ⁵¹A. Momeni, S. Baouche, L. Amiaud, F. Dulieu, J. H. Fillion, and J. L. Lemaire (unpublished).
- ⁵²H. Schlichting and D. Menzel, *Rev. Sci. Instrum.* **64**, 2013 (1993).
- ⁵³I. Engquist, I. Lundström, and B. Lieberg, *J. Phys. Chem.* **99**, 12257 (1995).
- ⁵⁴V. Buch and J. P. Devlin, *J. Chem. Phys.* **98**, 4195.
- ⁵⁵A. M. Jong and J. W. Niemantsverdriet, *Surf. Sci.* **233**, 355 (1990).
- ⁵⁶T. R. Govers, L. Mattera, and G. Scoles, *J. Chem. Phys.* **72**, 5446 (1980).
- ⁵⁷T. R. Govers (unpublished); available at <http://hal.ccsd.cnrs.fr/ccsd-00004273/en/>
- ⁵⁸J. P. Devlin and V. Buch, *J. Phys. Chem. B* **101**, 6095 (1997).
- ⁵⁹C. Manca, C. Martin, A. Allouche, and P. Roubin, *J. Phys. Chem. B* **105**, 12861 (2001).